Design of Backstepping Controller for PV-Wind Hybrid System with Grid-interfacing and Shunt Active Filtering Functionality

Jayasankar V N*, Vinatha U

Department of Electrical and Electronics,
National Institute of Technology Karnataka, Surathkal,
Srinivasanagar, Mangalore,
Karnataka -575025, India
E-mail: jayasankarvn@gmail.com
E-mail: u_vinatha@yahoo.co.in
*Corresponding author

Abstract: This paper presents the design of a double loop controller for the grid interconnection of PV-Wind hybrid system with shunt active filtering and neutral current compensation capabilities. Using Lypunov stability theory based procedure, a backstepping controller is designed for the outer loop dc link voltage control. The adaptive nature of back stepping controller results in better dynamic performance compared to conventional controllers. Inner loop consists of instantaneous power theory based controller for harmonic current compensation. Instantaneous power theory is modified by employing positive sinusoidal sequence regulator and self tuning filter to improve the system performance in unbalanced and distorted grid voltage conditions. A dynamic model of the system is considered for the design. Numerical simulations are done in MATLAB/Simulink platform for different system conditions to verify the effectiveness of controller in grid interfacing of renewable sources, and the shunt active filtering.

Keywords: Wind-solar hybrid system; Grid connected renewable system; Shunt Active Filter; Back-stepping control; DC Link voltage control.

Reference to this paper should be made as follows: Jayasankar V N, Vinatha U (2018), 'Design of Backstepping Controller for PV-Wind Hybrid System with Grid-interfacing and Shunt Active Filtering Functionality', *Int. J. of Power Electronics*, Vol.9, No.2, pp.167–188.

Biographical notes: Jayasankar V N received his B.Tech in Electrical & Electronics Engineering from Kannur University, India in 2010, M.Tech degree in Power Systems from National Institute of Technology Calicut, India in 2012. He is currently a PhD research fellow in National Institute of Technology Karnataka Surathkal, India. His research interests include renewable energy, power electronics and power quality.

Vinatha U received her B.Tech in Electrical & Electronics Engineering from KREC Surathkal, Mangalore University in 1986, M.Tech in Industrial Electronics from KREC Surathkal, Mangalore University in 1992, and the PhD in Electrical Engineering from National Institute of Technology Karnataka Surathkal, India in 2013. She is currently an Associate Professor in National Institute of Technology Karnataka Surathkal, India. Her research interests include power electronics and

drives, power electronic converters in renewable systems, mutilevel inverters, wave energy conversion system. She is a senior IEEE member.

1 Introduction

World's increasing energy demand and exhausting fossil fuels lead to the exploration of alternative energy resources for power generation. Wind and solar are two rapidly growing technologies for renewable power generation. Grid connection of wind and solar hybrid systems can be done using AC-shunted and DC-shunted topologies. With reference to Chen et al. (2006), latter topology is preferable as it reduces the number of grid interfacing inverters needed. The increasing use of unbalanced loads and non-linear loads in industrial and residential applications causes serious power quality problems. Use of active power filters is a solution for this problem. If a grid interfacing voltage source inverter itself gets additional functionality of a shunt active filter, the grid interconnection of renewable sources and power quality problem mitigation can be done using a single inverter, which yields reduction in overall cost of the system.

The grid interfacing inverter control strategy has mainly two cascaded loops. A faster inner loop controls the current to the grid, and a slower voltage loop controls the voltage at DC link. The current loop is for harmonic elimination, and current balancing, whereas voltage loop is for balancing the power flow to the grid. Several inverter control methods are proposed for shunt active filter as well as renewable energy grid integration.

Akagi et al. (1984) proposed 'instantaneous reactive theory' to calculate the reference current for the inner loop control. An alternative method using 'synchronous reference frame' is suggested by Bhattacharya and Divan (1995). Another method of inner loop control is 'peak detection method'. Cardenas et al. (2003) compared 'instantaneous power method', 'synchronous reference frame method' and 'peak detection method' and concluded that, under unbalance or distortions in grid voltage conditions, 'synchronous reference frame' is superior to others. But use of Phase locked loop is necessary in synchronous reference frame method. Abdusalam et al. (2008) proposed a 'modified instantaneous reactive power theory', in which low pass filters are replaced by 'self-tuning filters'. Self-tuning filters improve the dynamic performance and avoid the phase lag in filtering.

Akagi (2005) proposed a 'PI controller'-based DC link voltage control method. The error between reference value and DC link voltage value is processed in 'PI controller' and thus DC voltage is controlled. Mikkili and Panda (2011) suggested an 'adaptive fuzzy controller' for DC voltage control. Under balanced, unbalanced and distorted grid voltage conditions, 'adaptive fuzzy controller' was found to be superior to 'PI controller'. 'Backstepping controller' for DC link voltage regulation of shunt active filter is proposed by Ghamri et al. (2015). 'Backstepping controller' offers better dynamic performance under load variations, compared to others according to the literature.

Pulse generation methods for inverter are of two types; linear and non-linear techniques. 'Proportional Resonant control (PR)' proposed by Fukuda and Yoda (2001) is a linear technique. The main disadvantage of this technique is that multiple harmonics compensation is difficult to achieve using PR controller, because each harmonic component need individual resonant compensator, tuned at that particular harmonic frequency which

makes the system complex to implement. 'Proportional Integral Control (PI)' is a linear gating signal generation technique, proposed by Amin and Aliakbar (2007). The main drawback of PI method is high frequency harmonic oscillations. Another linear technique for gating signal generation is 'Repetitive Control (RC)' method. According to Chen et al. (2007), slow dynamic response is the main drawback of RC. Jeong and Seung (1997) proposed a non-linear 'predictive control' technique. The main disadvantage of 'predictive control' is that, in this method; the execution time of the control loop is large. Another non-linear technique, proposed by Malesani et al. (1998) is 'dead beat control', which is faster and simpler compared to 'predictive control'. 'Hysteresis control', proposed by Ingram and Round (1997) is a non-linear technique, in which the inverter follows a reference current by controlling the switches asynchronously. This method is simple and easy to implement.

In this paper, a new control strategy is proposed for the grid integration of renewable sources with power quality problem mitigation. Backstepping control algorithm is employed in outer loop for DC link voltage regulation. Instantaneous power theory is suggested for inner current loop. The performance of instantaneous power theory-based inner loop is found non satisfactory under unbalanced and distorted grid voltage conditions. So the instantaneous theory is modified by employing self-tuning filter and a positive sinusoidal signal regulator, so that reference current generation is not affected by distortions or unbalance in grid voltage. Hysteresis control is used for gating pulse generation. The proposed controller is designed to offer good dynamic performance and good power quality problem mitigation under different operating conditions. The simulations are done with the proposed control strategy for both unbalanced and distorted grid voltage conditions to verify the mentioned claims. Dynamic behaviour of the system is analysed by simulating step change in load, step change of wind speed and step change of solar irradiation.

2 System descriptions

The overall framework of a grid connected wind–solar hybrid system with non-linear load at 'the point of common coupling' is shown in Figure 1, which consists of a wind farm, solar PV array, an uncontrolled rectifier to convert generated AC in wind generator to DC, a DC–DC boost converter to keep the DC voltage at DC link bus voltage, a DC link capacitor, a voltage source inverter to invert the DC to AC, and AC filter. The detailed descriptions about different components are given below.

2.1 Wind farm

Wind farm consists of wind turbine coupled with a generator. By referring to Anderson and Bose (1983), the power generated by a wind turbine P_w can be expressed as shown in (1).

$$P_{wind} = 0.5\rho C_P A v_{wind}^3 \tag{1}$$

where P_{Wind} = Power generated by wind turbine (W), η = Turbine efficiency (%), ρ = Air density (kg/m^3), C_P = Power Co-efficient, A = Rotor area (m^2), v_{wind} = Velocity of wind (m/s), ω_w = Turbine rotor speed (rad/s).

The mechanical energy generated by wind turbine is converted to electrical energy using a generator. With reference to Wang et al. (2012), it can be stated that 'doubly fed

induction generators (DFIG)', 'fixed speed induction generators (FSIG)', and 'permanent magnet induction generators (PMSG)' are the commonly used generators in wind farms. PMSG is used in this study. As the operating frequency of PMSG is decoupled from the grid frequency, maximum power can be extracted using maximum power point tracking methods. PMSG has no gear boxes attached, so the overall weight is reduced and the efficiency is higher compared to the other alternatives.

Figure 1 Overall block diagram of grid connected wind–solar system

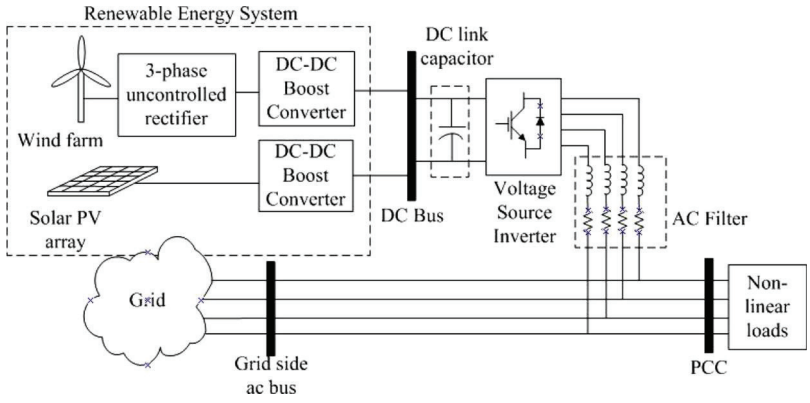

The generator output is rectified using an uncontrolled three-phase rectifier. The rectifier output is connected to a DC–DC boost converter to keep the output voltage constant (Jayasankar and Vinatha, 2016).

2.2 Solar PV System

Solar PV system consists of PV arrays connected in series and parallel. The solar PV system can be modelled as a current source as expressed in (2) (Gow and Manning, 1996; Villalva et al., 2009). Modelling of solar PV array is explained in more detail by Jayasankar et al. (2016). The solar PV output is connected to the common DC bus through a DC–DC boost converter, which maintains the output voltage constant.

$$I_m = N_P I_{PV} - N_P I_0 exp\left[\frac{V + IR_s(N_s/N_p)}{N_S V_t a} - 1\right] - \left[\frac{V + IR_s(N_s/N_p)}{R_P(N_s/N_p)}\right] \quad (2)$$

where N_p = Number of parallel cells, N_s = Number of series cells, I_{PV} = Photovoltaic Current, I_0 = Saturation Current, V_t = Thermal Voltage of the cell, a = Diode constant ($1 \leq a \leq 1.5$), R_s = Series resistance of PV cell, R_p = Shunt resistance of PV cell.

2.3 DC link capacitor

DC link capacitor is used for reducing the DC ripple. It also acts as an energy storage element during transients. Larger the DC capacitor value, smaller the ripple. As the size of the capacitor increases, the response time of the system to power changes increases. If DC capacitor value is small, faster the response to power changes, but high voltage ripples on

DC side. Chaoui et al. (2008) proposed a formula for calculating optimum DC capacitor value as shown in (3):

$$C_{dc} \geq \frac{2E_{max}}{V_{dc}^2 - V_{dcmin}^2} \tag{3}$$

where E_{max} is the maximum energy that the capacitor has to supply during transient condition.

2.4 Voltage source inverter

Three phase four leg voltage source inverter plays mainly three roles in the system: one is to inject power generated by renewable sources to grid; another to maintain the power quality at the distribution system; and the third role is to balance the load by neutral current compensation. The inverter consists of eight IGBT switches and anti-parallel diodes. The main objective of the work presented in this paper is to design the controller for the inverter switch control with grid interfacing and shunt active filtering capabilities.

2.5 AC filter

The currents and voltages at the AC side of the inverter consists of higher order harmonics and switching frequency components. AC filters are used to filter out the unwanted frequency components. Inductive filters are used in this study. The filter inductance can be calculated using (4):

$$L_c = \frac{V_{dc}}{6 f_c \Delta I_{ppmax}} \tag{4}$$

where ΔI_{ppmax} is the maximum ripple current, f_c, the switching frequency and V_{dc} is the DC link voltage.

3 Control system design

The schematic diagram of the control system is shown in Figure 2. The control objectives are, filtering of harmonic currents and DC voltage control.

3.1 Harmonic current extraction

Harmonic current extraction is done using modified pq theory. The grid side voltages (v_s^a, v_s^b, v_s^c) and load currents (i_L^a, i_L^b, i_L^c) are transformed into $\alpha\beta$ frame as shown in (5) and (6). Where v_s^α, v_s^β and i_L^α, i_L^β are grid voltages and load currents in $\alpha\beta$ frame, respectively .

$$\begin{bmatrix} v_s^\alpha \\ v_s^\beta \end{bmatrix} = \sqrt{\frac{2}{3}} \begin{bmatrix} 1 & -\frac{1}{2} & -\frac{1}{2} \\ 0 & \frac{\sqrt{3}}{2} & -\frac{\sqrt{3}}{2} \end{bmatrix} \begin{bmatrix} v_s^a \\ v_s^b \\ v_s^c \end{bmatrix} \tag{5}$$

$$\begin{bmatrix} i_L^\alpha \\ i_L^\beta \\ i_L^0 \end{bmatrix} = \sqrt{\frac{2}{3}} \begin{bmatrix} 1 & -\frac{1}{2} & -\frac{1}{2} \\ 0 & \frac{\sqrt{3}}{2} & -\frac{\sqrt{3}}{2} \\ \frac{1}{\sqrt{2}} & \frac{1}{\sqrt{2}} & \frac{1}{\sqrt{2}} \end{bmatrix} \begin{bmatrix} i_L^a \\ i_L^b \\ i_L^c \end{bmatrix} \tag{6}$$

A positive sequence signal regulator (PSSR), proposed by Yavari et al. (2012), is employed in the controller to identify the fundamental positive sequence components of grid voltages. A sinusoidal signal integrator (SSR) is the main part of PSSR. The input to PSSR is grid voltage signals in $\alpha\beta$ frame. The fundamental positive sequence components of the grid voltages are having the angular frequency equal to resonance frequency (ω) of SSR. Therefore, the positive sequence components are instantaneously integrated. When the input signal frequency is not equal to the resonance frequency of SSR, the integration output will be zero. A negative feedback loop to the SSR makes it a regulator, which can identify the fundamental component of positive sequence signal from the input signal. The schematic diagram of PSSR is shown in Figure 3. v_{sp1}^{α} and v_{sp1}^{β} are the fundamental positive sequence components of grid voltage in $\alpha\beta$ frame. The constant K is sensitivity constant, which controls the response time and bandwidth of PSSR.

Figure 2 Schematic diagram of control system

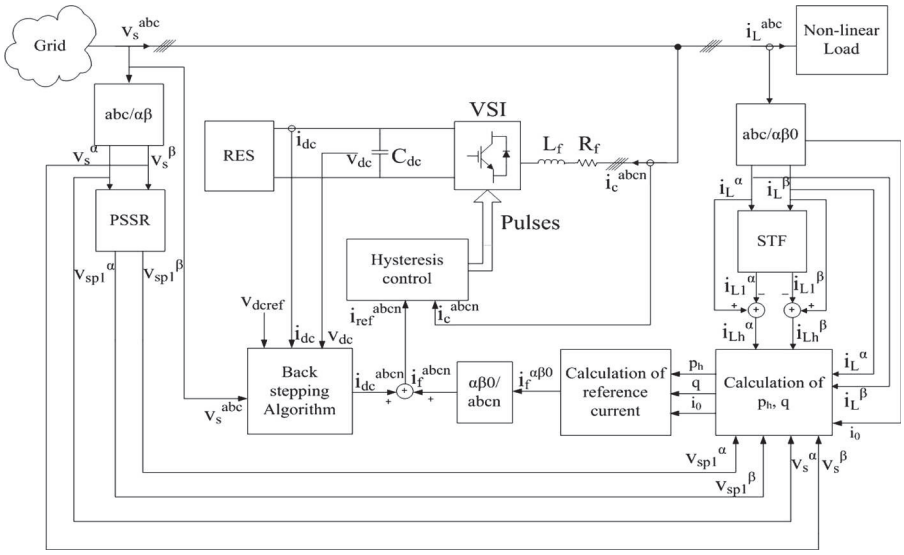

Figure 3 Schematic diagram of PSSR

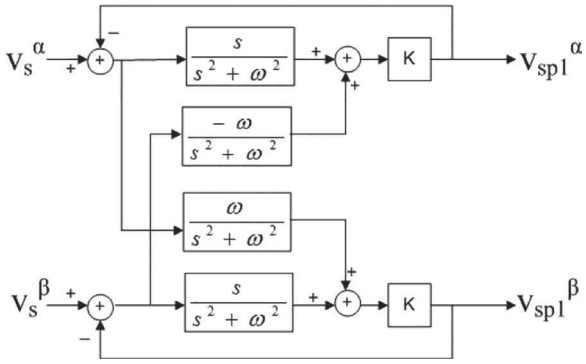

A self-tuning filter (STF) is employed to find the fundamental components of load currents. According to Benchouia et al. (2015), STF extracts the fundamental components at the frequency ω , and suppresses all other harmonic components. The schematic diagram of STF is shown in Figure 4. The fundamental components of load current in $\alpha\beta$ frame are represented as i_{L1}^{α} and i_{L1}^{β}. The harmonic components of load currents, i_{Lh}^{α} and i_{Lh}^{β} can be calculated by subtracting fundamental component of load current (i_{L1}^{α} and i_{L1}^{β}) from total load current (i_{L}^{α} and i_{L}^{β}).

Figure 4 Schematic diagram of STF

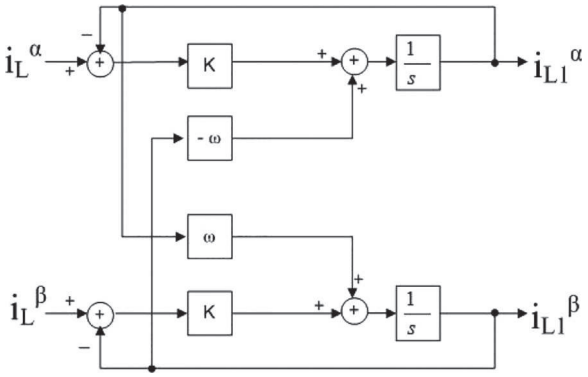

Instantaneous active power for harmonic current compensation $p_h(t)$ and instantaneous imaginary power $q(t)$ are calculated as shown in Eqs. (7) and (8):

$$p_h(t) = i_{Lh}^{\alpha} v_{sp1}^{\alpha} + i_{Lh}^{\beta} v_{sp1}^{\beta} \tag{7}$$

$$q(t) = i_{L}^{\beta} v_{s}^{\alpha} - i_{L}^{\alpha} v_{s}{}^{\beta} \tag{8}$$

The filter currents in $\alpha\beta$ frame are calculated using equation (9). The negative sign in (9) represents a phase difference of 180^0, as the inverter currents have to cancel out the harmonic components at PCC:

$$\begin{bmatrix} i_f{}^{\alpha} \\ i_f{}^{\beta} \\ i_f{}^{0} \end{bmatrix} = -\frac{1}{(v_{sp1}^{\alpha})^2 + (v_{sp1}^{\beta})^2} \begin{bmatrix} v_{sp1}^{\alpha} & -v_{sp1}^{\beta} & 0 \\ v_{sp1}^{\beta} & v_{sp1}^{\alpha} & 0 \\ 0 & 0 & (v_{sp1}^{\alpha})^2 + (v_{sp1}^{\beta})^2 \end{bmatrix} \begin{bmatrix} p_h \\ q \\ i_0 \end{bmatrix} \tag{9}$$

The filter currents in abc frame are calculated using (10). The neutral current can be calculated using (11):

$$\begin{bmatrix} i_f^a \\ i_f^b \\ i_f^c \end{bmatrix} = \sqrt{\frac{2}{3}} \begin{bmatrix} 1 & 0 & \frac{1}{\sqrt{2}} \\ -\frac{1}{2} & \frac{\sqrt{3}}{2} & \frac{1}{\sqrt{2}} \\ -\frac{1}{2} & -\frac{\sqrt{3}}{2} & \frac{1}{\sqrt{2}} \end{bmatrix} \begin{bmatrix} i_f^{\alpha} \\ i_f^{\beta} \\ i_f^0 \end{bmatrix} \tag{10}$$

$$i_f^n = i_f^a + i_f^b + i_f^c \tag{11}$$

3.2 DC voltage control

For satisfactory performance under dynamically changing system conditions, DC voltage controller can be designed using back stepping algorithm. It is a non-linear control algorithm, where Lyapunov theory of stability is used for deriving the control law. According to Lypunov theory,

"A system is stable at the point x if there is a function continually derivable $U(x)$ that satisfy:
$U(0) = 0$
$U(x) > 0; \forall x \neq 0, x \in \Omega$
$\dot{U}(x) < 0; \forall x \neq 0, x \in \Omega$; Where Ω is the domain of study " (Ghamri et al., 2015).

Energy stored in DC link capacitor can be written as a function of v_{dc} as shown in (12):

$$E_{dc} = \frac{1}{2} C_{dc} V_{dc}^2 \tag{12}$$

The derivative of E_{dc} can be written as shown in (13):

$$\dot{E_{dc}} = P_{dc} = P_s + P_{RES} - P_{Rdc} - P_{sw} \tag{13}$$

P_s is the power supplied by the network to maintain the charge in DC link capacitor, P_{RES} is the power injected by renewable sources, P_{Rdc} is the losses in leakage resistance of DC link capacitor, , and P_{sw} is the inverter switching loss. Mathematical models of P_s, P_{Rdc} and P_{RES} are shown in (14)–(16), respectively. P_{sw} is treated as an unknown parameter:

$$P_s = v_s^a i_{dc}^a + v_s^b i_{dc}^b + v_s^c i_{dc}^c \tag{14}$$

where v_s^a, v_s^b and v_s^c are the three phase grid voltages and i_{dc}^a, i_{dc}^b and i_{dc}^c are the three phase inverter current components for DC voltage control:

$$P_{RES} = i_{dc} v_{dc} \tag{15}$$

$$P_{Rdc} = \frac{v_{dc}^2}{R_{dc}} \tag{16}$$

where i_{dc} is the DC current from RES to DC link capacitor and R_{dc} is the leakage resistance of DC capacitor.

The control objective is to keep the DC voltage tracking error as small as possible. If z is the voltage tracking error, it can be represented as shown in (17):

$$z = x^* - x \tag{17}$$

where x is energy stored in DC capacitor and x^* is the reference value of energy stored in DC link voltage. The derivative of (17) can be written as shown in (18):

$$\dot{z} = \dot{x^*} - \dot{x} = \dot{x^*} - P_s - P_{RES} + P_{Rdc} + P_{sw} \tag{18}$$

From (12), (15) and (16); Eq. (18) can be rewritten as (19):

$$\dot{z} = \dot{x^*} - P_s - i_{dc}\sqrt{\frac{2x}{C_{dc}}} + \frac{2x}{C_{dc} R_{dc}} + P_{sw} \tag{19}$$

For obtaining a stabilized control law, introducing a Lyapunov function as shown in (20):

$$V = \frac{1}{2}z^2 + \frac{1}{2\gamma}\tilde{P_{sw}}^2 \tag{20}$$

Where $\tilde{P_{sw}}$ is the estimation error of P_{sw} and γ is a positive design parameter. Differentiating (20), we get (21):

$$\dot{V} = z\dot{z} + \frac{1}{\gamma}\tilde{P_{sw}}\dot{\tilde{P_{sw}}} \tag{21}$$

Substituting (19) in (21), Eq. (22) can be derived:

$$\dot{V} = z(\dot{x^*} - P_s - i_{dc}\sqrt{\frac{2x}{C_{dc}}} + \frac{2x}{C_{dc}R_{dc}} + \hat{P_{sw}}) + \frac{1}{\gamma}\tilde{P_{sw}}\dot{\tilde{P_{sw}}} \tag{22}$$

Equation (23) represents the control law derived from (22). Equation (24) represents the parameter adaptation law:

$$P_s = \dot{x^*} - i_{dc}\sqrt{\frac{2x}{C_{dc}}} + \frac{2x}{C_{dc}R_{dc}} + \hat{P_{sw}} + cz \tag{23}$$

$$\dot{\tilde{P_{sw}}} = \gamma z \tag{24}$$

Equation (25) can be derived from (14) and (23). The inverter current references for DC voltage control can be calculated using (25):

$$\begin{bmatrix} i_{dc}^a \\ i_{dc}^b \\ i_{dc}^c \end{bmatrix} = \frac{1}{(v_s^a)^2 + (v_s^b)^2 + (v_s^c)^2} \begin{bmatrix} v_s^a(\dot{x^*} - i_{dc}\sqrt{\frac{2x}{C_{dc}}} + \frac{2x}{C_{dc}R_{dc}} + \hat{P_{sw}} + cz) \\ v_s^b(\dot{x^*} - i_{dc}\sqrt{\frac{2x}{C_{dc}}} + \frac{2x}{C_{dc}R_{dc}} + \hat{P_{sw}} + cz) \\ v_s^c(\dot{x^*} - i_{dc}\sqrt{\frac{2x}{C_{dc}}} + \frac{2x}{C_{dc}R_{dc}} + \hat{P_{sw}} + cz) \end{bmatrix} \tag{25}$$

The neutral current can be calculated using (26).

$$i_{dc}^n = i_{dc}^a + i_{dc}^b + i_{dc}^c \tag{26}$$

The closed loop DC voltage control equation is given by (27):

$$\begin{bmatrix} \dot{z} \\ \dot{\tilde{P}}_{sw} \end{bmatrix} = \begin{bmatrix} -c & -1 \\ \gamma & 0 \end{bmatrix} \begin{bmatrix} z \\ \tilde{P}_{sw} \end{bmatrix} \tag{27}$$

According to Lyapunov's theory, system is stable if $\dot{z}$ and $\dot{\tilde{P}}_{sw}$ has negative real value, which implies $c^2 - 4\gamma > 0$. Since there are no systematic ways in non-linear control to make suitable choices of c and γ, trial and error method can be used to find c and then parameter γ can be selected using the inequality $c^2 - 4\gamma > 0$.

3.3 Reference current calculation and gating signal generation

The reference currents for the inverter is the sum of i_f^{abcn} and i_{dc}^{abcn} as shown in (28).

$$\begin{bmatrix} i_{ref}^a \\ i_{ref}^b \\ i_{ref}^c \\ i_{ref}^n \end{bmatrix} = \begin{bmatrix} i_f^a \\ i_f^b \\ i_f^c \\ i_f^n \end{bmatrix} + \begin{bmatrix} i_{dc}^a \\ i_{dc}^b \\ i_{dc}^c \\ i_{dc}^n \end{bmatrix} \tag{28}$$

Hysteresis controller compares the reference currents with the inverter currents in real time. If the error signals exceeds the upper band limit, the upper switch in the inverter leg is turned off and lower switch is turned on. Similarly, if the error is less than the lower band limit, the upper switch is turned on and lower switch is turned off. Figure 5 shows the operation of hysteresis controller.

Figure 5 Working of hysteresis controller

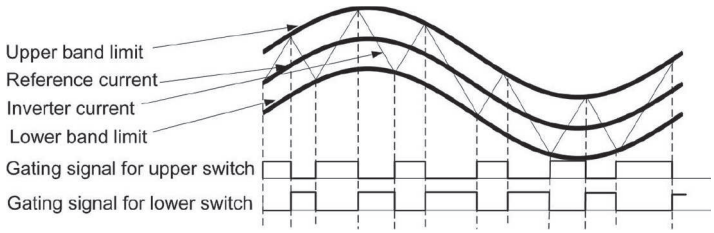

4 Simulations and discussion

In simulations, the wind and solar dynamic models are connected to the power grid using a three phase four leg IGBT inverter. A wind turbine of tower height 30 m and rotor diameter 51.2 m and solar cells of open circuit voltage 21.1 V and short circuit current 3.8 A are considered for simulation. The system parameters are listed in Table 1.

Table 1 System parameters

S. no.	*Particulars*	*Values*
1	Supply voltage	230 V rms (phase - neutral), 50 Hz
2	Source parameters	0.01 mH, 0.1 Ω
3	DC link capacitance	2350 μF
4	DC link voltage	700 V
5	Filter Parameters	5 mH, 0.1 Ω
6	Load parameters	20 Ω, 60 mH

The effectiveness of proposed controller is examined by carrying out the simulations for different cases. The control gains for the back stepping controller are, $c = 500$, $\gamma = 40{,}000$. The simulations for different cases are presented in Figures 6–22.

Figure 6 DC link voltage plot and power plots for case 1. (a) DC link voltage, (b) power from grid, (c) power from renewable sources and (d) load power (see online version for colours)

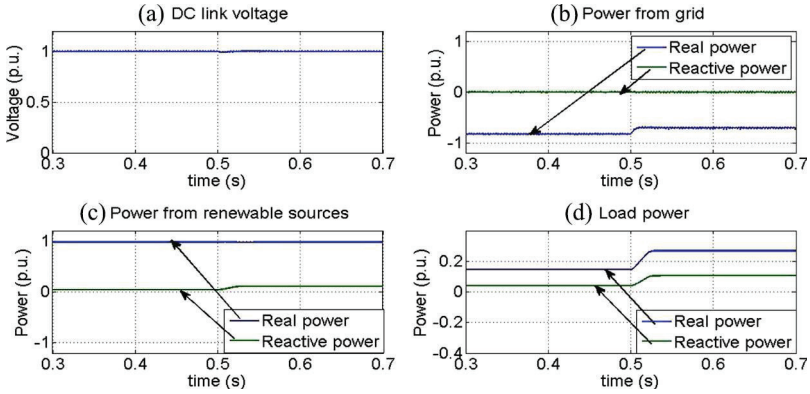

4.1 Case 1: a step change of load current

A step increment of load current by 50% at 0.5 s is simulated. Figures 6 and 7 are the simulation results for case 1. Figure 6a is the DC link voltage, Figure 6b–d are the power from grid side, power from renewable sources, and power at load, respectively. The power from grid is negative, because power flows to the grid from renewable sources. At 0.5 s, the load increases by 50%. The real power flow to the grid reduces, as renewable source supplies the increased power demand of the load. The increased reactive power demand is entirely drawn from renewable sources as shown in Figure 6c.

Figures 7a–c are the load current for phase A, inverter current for phase A, and grid voltage and current for phase A, respectively. Figure 7d is the zoomed in version of 7c, which shows the decrement in grid current as load increases at 0.5 s. The inverter current cancels out the harmonic currents and grid current maintains its sinusoidal shape.

Figure 7 Current and voltage plots for case 1. (a) Load current, (b) inverter current, (c) grid voltage and current of phase A and (d) grid voltage and current of phase A (see online version for colours)

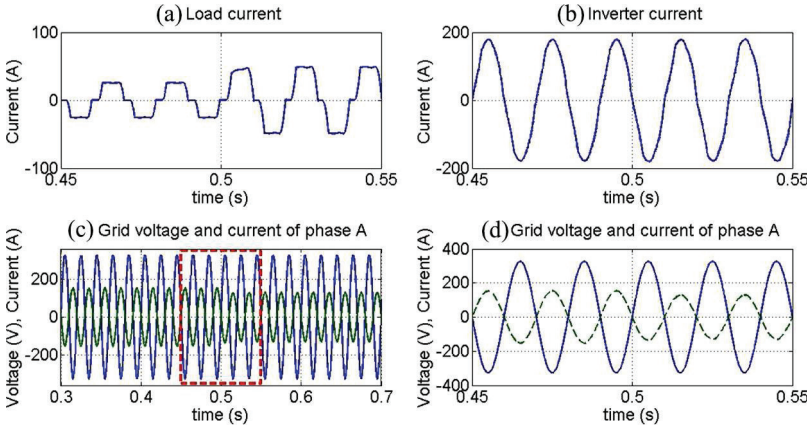

Figure 8a and b shows the harmonic spectrum of phase A load current and grid current. The load current THD is 18.91% and the grid current THD is 1.32%.

Figure 8 Harmonic spectrum of load current and grid current for case 1. (a) Phase A load current harmonic spectrum and phase A grid current harmonic spectrum (see online version for colours)

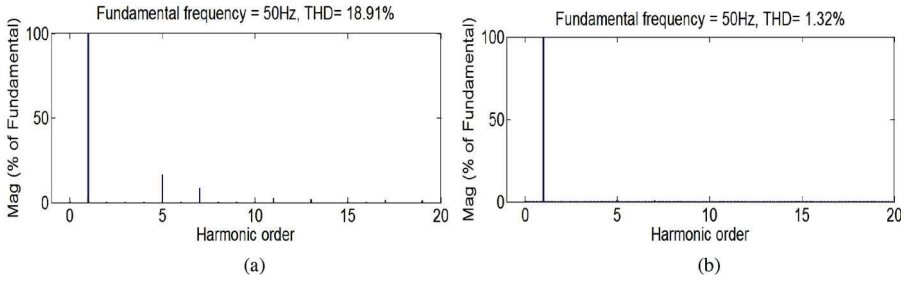

4.2 Case 2: a step change of wind speed and solar irradiation

A step change of wind speed from 12 to 6 m/s at 0.4 s, and step change of solar irradiation from 1 to 0.5 $\mathrm{kWh/m^2}$ at 0.8 s. is simulated. DC link voltage is maintained constant at 1 p.u. as shown in Figure 9a. As the power generation from renewable sources decreases, the power flow to grid decreases as shown in Figure 9b and c. The load demand is constant as shown in Figure 9d; the real and the reactive power demand of the load is supplied by renewable sources, and the excess power is fed to the grid.

Figure 9 DC link voltage plot and power plots for case 2. (a) DC link voltage, (b) power from grid, (c) power from renewable sources and (d) load power (see online version for colours)

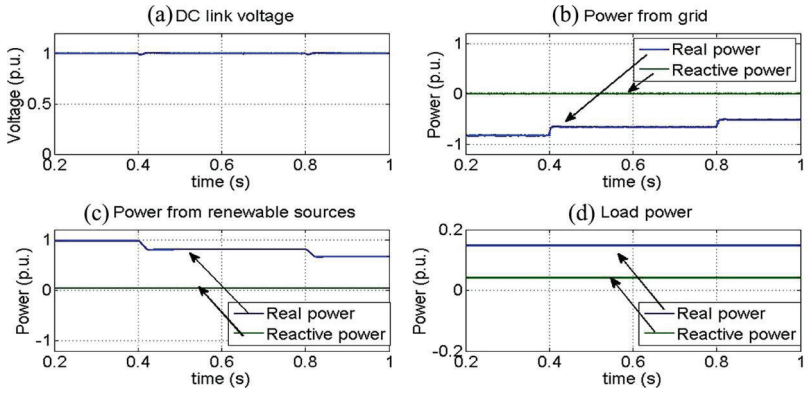

Figure 10 shows the current and voltage plots. For a constant load current, the current to grid decreases as the inverter current decreases due to decrement in renewable power generation.

Figure 11a and b shows the harmonic spectrum of phase A load current and grid current. The load current THD is 22.29% and the grid current THD is 1.02%.

Figure 10 Current and voltage plots for case 2. (a) Load current, (b) inverter current, (c) grid voltage and current of phase A, (d) grid voltage and current of phase A, (e) grid voltage and current of phase A and (f) grid voltage and current of phase A (see online version for colours)

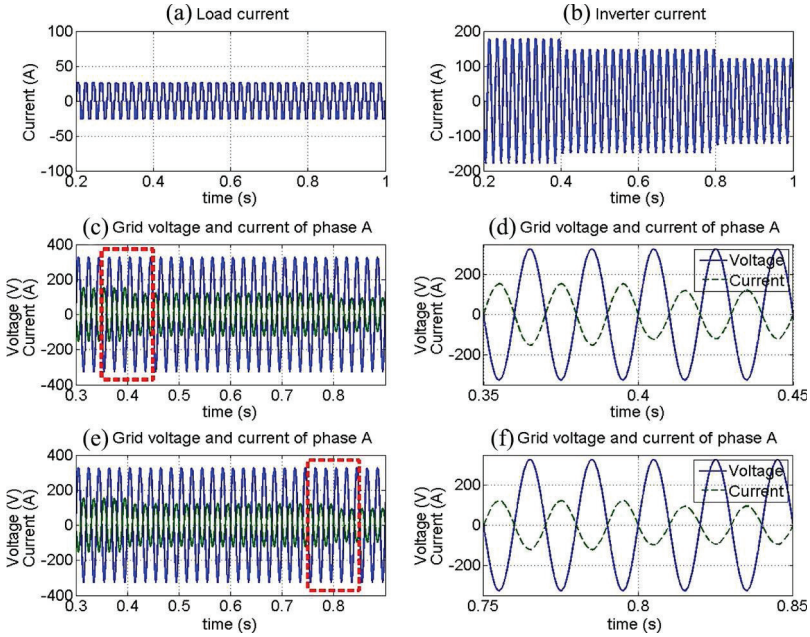

Figure 11 Harmonic spectrum of load current and grid current for case 2. (a) Phase A load current harmonic spectrum and (b) phase A grid current harmonic spectrum (see online version for colours)

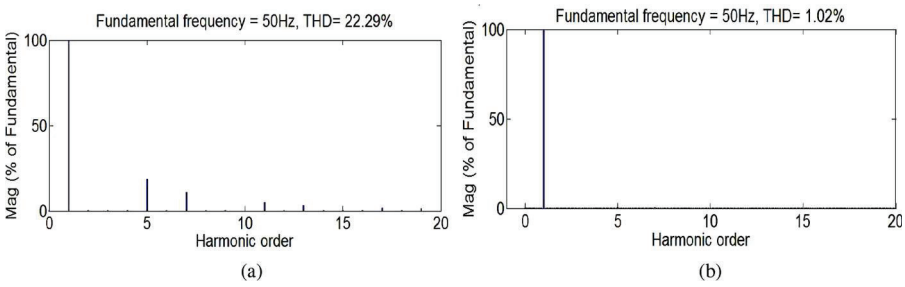

4.3 Case 3: renewable generation becomes zero

Renewable generation is forced to zero at 0.5 s. Figure 12a shows that the DC link voltage is constant at 1 p.u. Real power from grid becomes positive as shown in Figure 12b, as the load demand has to be completely met from the grid now. Figure 12c shows that even though real power supply from the renewable sources is zero, reactive power supplied by renewable sources is not zero. The real and reactive power demand of the load is shown in Figure 12d. It can be observed that the real power is supplied by the grid and reactive power is supplied by the grid interfacing inverter of renewable sources.

Figure 12 DC link voltage plot and power plots for case 3. (a) DC link voltage, (b) power from grid, (c) power from renewable sources and (d) load power (see online version for colours)

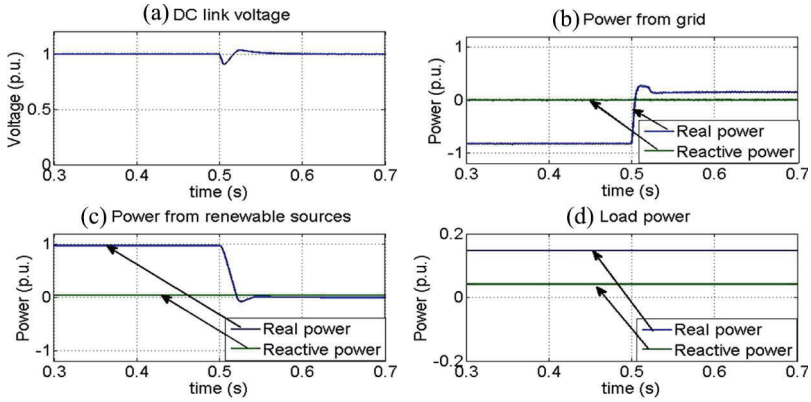

Figure 13a shows that the load current is maintained constant at 1 p.u. When renewable power generation is present, real power transfer, compensation of harmonic currents and reactive power compensation are the responsibilities of inverter. But when renewable power generation is zero, real power transfer by the inverter is also zero. Figure 13b shows that at 0.5 s, the shape of inverter current changes. The grid current direction gets reversed at 0.5 s due to the change in direction of power flow to the grid as shown in Figure 13c and d. The inverter current compensates the harmonic currents and maintains the sinusoidal shape of grid current.

Figure 13 Current and voltage plots for case 3. (a) Load current, (b) inverter current, (c) grid voltage and current of phase A and (d) grid voltage and current of phase A (see online version for colours)

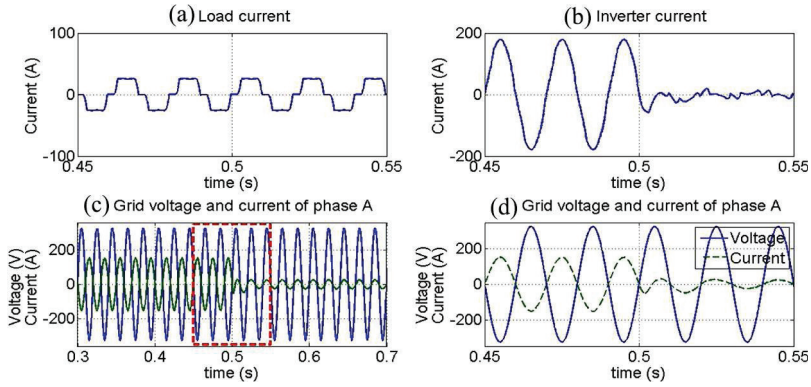

Figure 14a and b shows the harmonic spectrum of phase A load current and grid current. The load current THD is 22.29% and the grid current THD is 3.03%.

Figure 14 Harmonic spectrum of load current and grid current for case 3. (a) Phase A load current harmonic spectrum and (b) phase A grid current harmonic spectrum (see online version for colours)

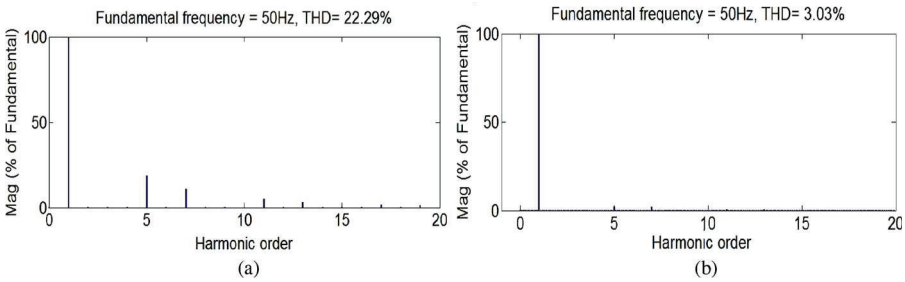

4.4 Case 4: distortion in grid voltage

A distorted grid voltage condition with 5% THD is simulated by injecting voltage harmonics at 0.5 s. DC link voltage is maintained constant by the controller in this case as in Figure 15a. Grid power flows remain unaltered as shown in Figure 15b. The real and reactive power flows from renewable sources are not affected by the distortions in grid voltage as shown in Figure 15c. Load demand is constant and balanced in this case as shown in Figure 15d.

Figure 15 DC link voltage plot and power plots for case 4. (a) DC link voltage, (b) power from grid, (c) power from renewable sources and (d) load power (see online version for colours)

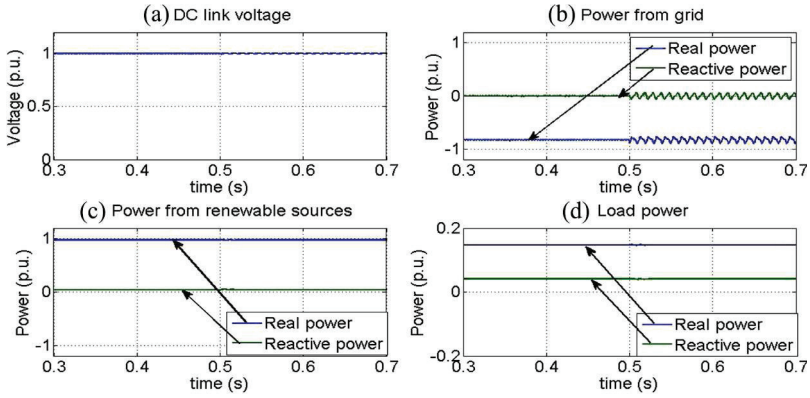

Figure 16 shows that the grid current magnitude and shape remain unaltered even in the presence of harmonics in grid voltage. Figure 17a, c and e shows the harmonic spectrum of phase A, phase B and phase C load currents, respectively. Figure 17b, d and f are the harmonic spectrum of phase A, phase B and phase C grid currents, respectively.

The load current THDs are 22.29% in all three phases and the grid current THDs are 0.65% in all three phases. So we can say that the controller satisfactorily works in distorted grid voltage condition.

Figure 16 Current and voltage plots for case 4. (a) Load current, (b) inverter current, (c) grid voltage and current of phase A and (d) grid voltage and current of phase A (see online version for colours)

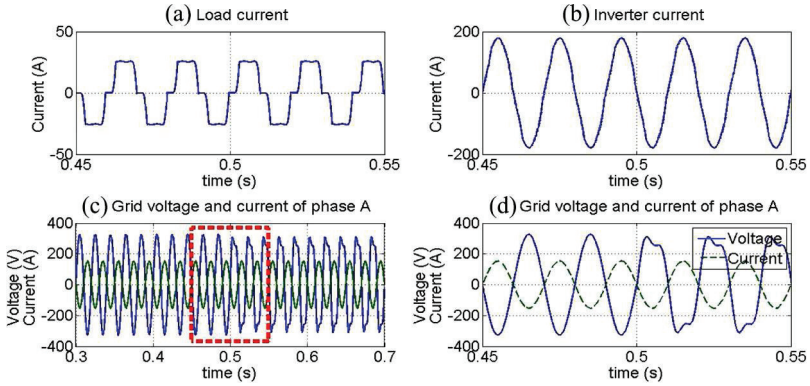

Figure 17 Harmonic spectrum of load currents and grid currents for case 4. (a) Phase A load current harmonic spectrum, (b) phase A grid current harmonic spectrum, (c) phase B load current harmonic spectrum, (d) phase B grid current harmonic spectrum, (e) phase C load current harmonic spectrum and (f) phase C grid current harmonic spectrum (see online version for colours)

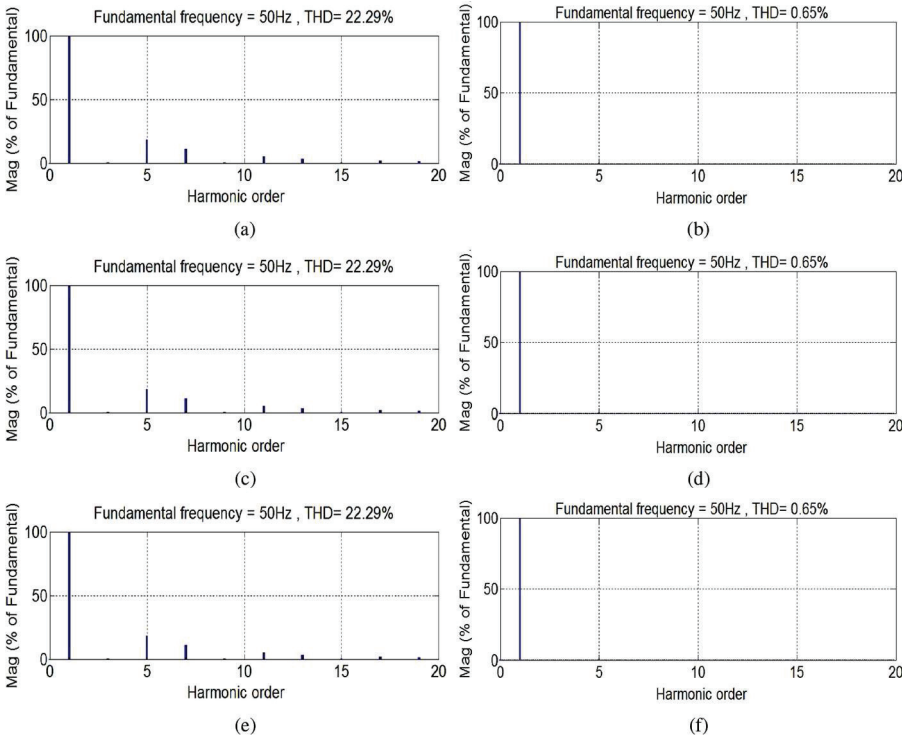

4.5 Case 5: unbalance in grid voltage

An unbalance in grid voltage is simulated by increasing the amplitude of phase A voltage by 20% at 0.5 s. DC link voltage remains same under balanced and unbalanced grid voltage conditions as in Figure 18a. From Figure 18b and c it can be observed that, even though unbalance is present in the grid voltage, power flows from renewable sources and grid have no significant variation. Load demand is constant and balanced as shown in Figure 18d. Figure 19 shows the current and voltage plots. The grid currents remain balanced and sinusoidal by the controller action.

Figure 18 DC link voltage plot and power plots for case 5. (a) DC link voltage, (b) power from grid, (c) power from renewable sources and (d) load power (see online version for colours)

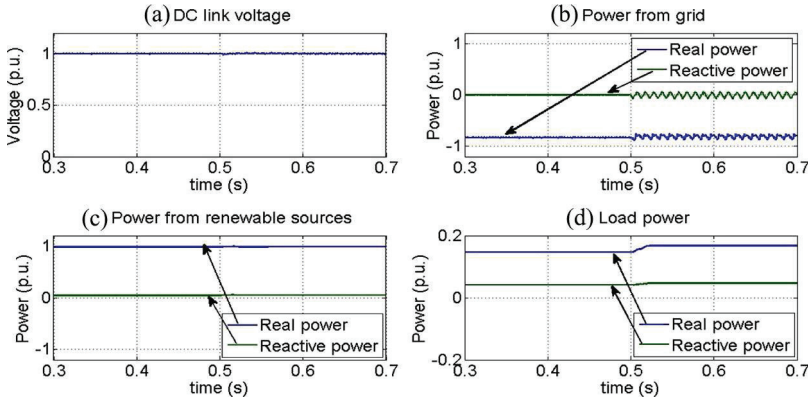

Figure 19 Current and voltage plots for case 5. (a) Load current, (b) inverter current, (c) three-phase grid voltage and (d) grid voltage and current of phase A (see online version for colours)

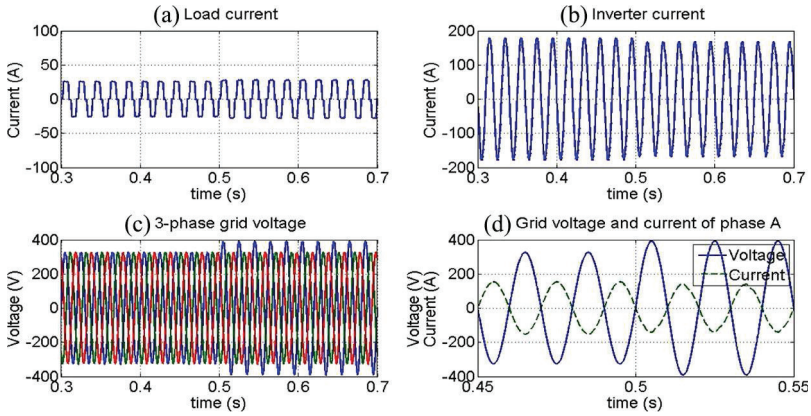

Figure 20a, c and e shows the harmonic spectrum of phase A, phase B and phase C load currents, respectively. Figure 20b, d and f are the harmonic spectrum of phase A, phase B and phase C grid currents, respectively.

The load current THDs are 20.46, 23.45 and 23.54% in phase A, phase B and phase C, respectively and the grid current THDs are 3.34, 1.65 and 3.39% in phase A, phase B and phase C, respectively. So it can be concluded that system works satisfactorily under unbalanced grid voltage condition.

Figure 20 Harmonic spectrum of load currents and grid currents for case 5. (a) Phase A load current harmonic spectrum, (b) phase A grid current harmonic spectrum, (c) phase B load current harmonic spectrum, (d) phase B grid current harmonic spectrum, (e) phase C load current harmonic spectrum and (f) phase C grid current harmonic spectrum (see online version for colours)

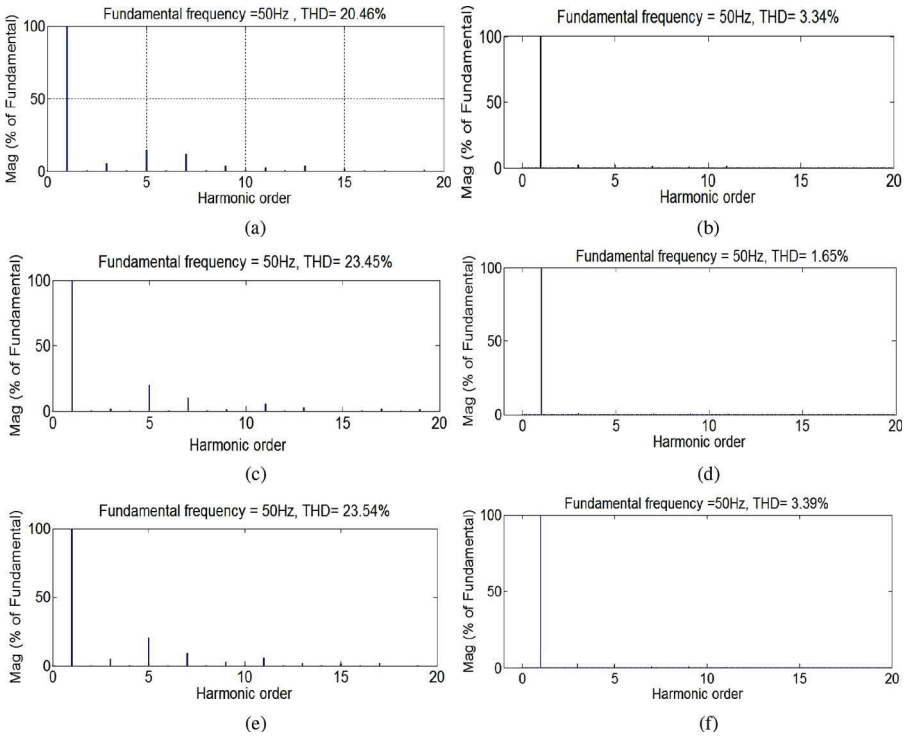

4.6 Case 6: unbalance in load

An unbalance is simulated in load by connecting a 20 Ω, 60 mH load between A phase and neutral, at 0.5 s. Renewable power generation is considered as constant in this case. Grid voltage is considered as balanced and un distorted. Figure 21 shows the DC link voltage and power plots for this case. Unbalance in load has not introduced any significant change in DC link voltage and power flows.

Figure 22 shows the voltage and current plots for case 6, from which it can be observed that the under unbalance in load currents, grid side currents remains balanced and sinusoidal. The fourth leg of inverter compensates the unbalance in load current.

Figure 23a, c and e shows the harmonic spectrum of phase A, phase B and phase C load currents, respectively. Figure 23b, d and f are the harmonic spectrum of phase A, phase B and phase C grid currents, respectively. The load current THDs are 16.19, 22.33 and

22.04% in phase A, phase B and phase C, respectively and the grid current THDs are 4.82, 4.92 and 1.05% in phase A, phase B and phase C, respectively.

Figure 21 DC link voltage plot and power plots for case 6. (a) DC link voltage, (b) power from grid, (c) power from renewable sources and (d) load power (see online version for colours)

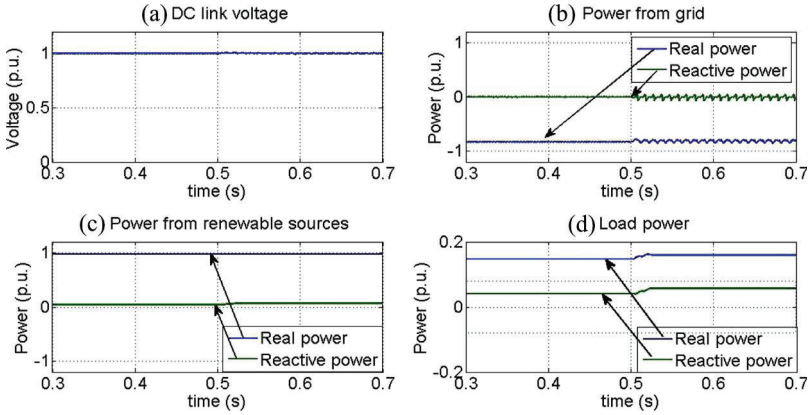

Figure 22 Current and voltage plots for case 6. (a) three-phase load current, (b) three-phase inverter current, (c) three-phase grid voltage and (d) three-phase grid current (see online version for colours)

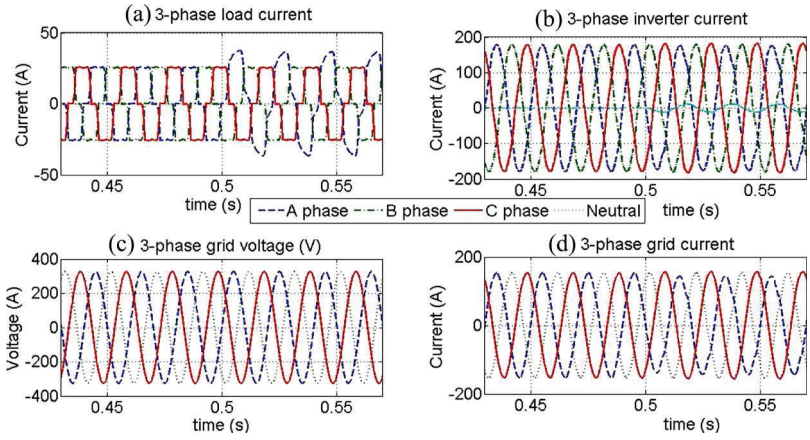

The grid current THD for all cases are listed in Table 2. The grid current THDs are below 5% in all cases, which is well within the harmonic limits recommended by IEEE 519-1992.

Figure 23 Harmonic spectrum of load currents and grid currents for case 6. (a) Phase A load current harmonic spectrum, (b) phase A grid current harmonic spectrum, (c) phase B load current harmonic spectrum, (d) phase B grid current harmonic spectrum, (e) phase C load current harmonic spectrum and (f) phase C grid current harmonic spectrum (see online version for colours)

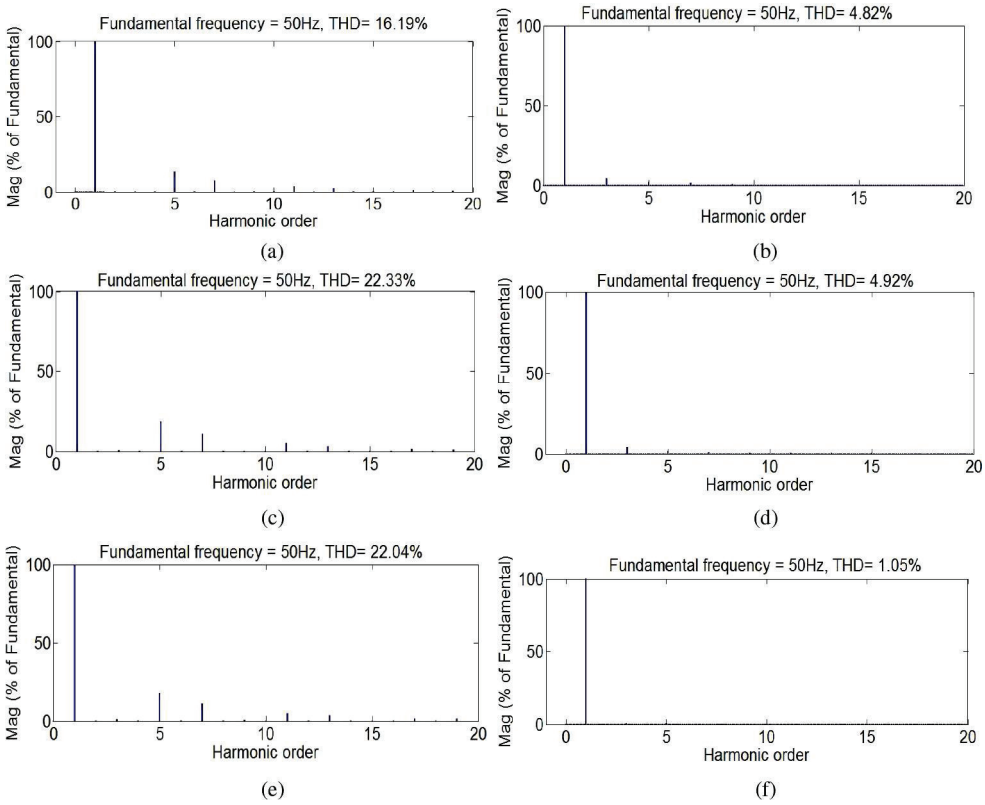

Table 2 Grid current and load current THD in %

	THD of grid current in %			*THD of load current in %*		
Simulation cases	*Phase A*	*Phase B*	*Phase C*	*Phase A*	*Phase B*	*Phase C*
Case 1	1.32	1.32	1.32	18.91	18.91	18.91
Case 2	1.02	1.02	1.02	22.29	22.29	22.29
Case 3	3.03	3.03	3.03	22.29	22.29	22.29
Case 4	0.65	0.65	0.65	22.29	22.29	22.29
Case 5	3.34	1.65	3.39	20.46	23.45	23.54
Case 6	4.82	4.92	1.05	16.19	22.33	22.04

5 Conclusion

A controller for grid interfacing inverter with shunt active filtering capability has been successfully designed in this study. The outer loop controller for DC link voltage control has been designed with back stepping algorithm using Lyapunov stability theory, whereas

inner current loop has been designed by modifying the instantaneous power theory for unbalanced and distorted grid voltage conditions. The power flow and harmonic analysis results shows that the controller works effectively under different cases simulated.

Major contributions of this study are,

i Successful utilization of back stepping algorithm for DC link voltage control.

ii Modification of instantaneous power theory by introducing positive sequence sinusoidal signal regulator (PSSR) and self-tuning filter (STF).

References

Abdusalam, M., Poure, P. and Saadate, S. (2008) 'Hardware implementation of a three-phase active filter system with harmonic isolation based on self-tuning-filter', in *PESC 2008: Proceedings of 39th IEEE Annual Power Electronics Specialists Conference*, 15–19 June 2008, Rhodes, Greece, Vol. 1, No. 1, pp.2875–2881.

Akagi, H. (2005) 'The state-of-the-art of active filters for power conditioning', in *2005 European Conference on Power Electronics and Applications*, 11–14 September 2005, Dresden, Germany, Vol. 1, No. 1, pp.1–15.

Akagi, H., Kanazawa, Y. and Nabae, A. (1984) 'Instantaneous reactive power compensators comprising switching devices without energy storage components', *IEEE Transactions on Industry Applications*, Vol. 20, pp.625–630.

Amin, H. and Aliakbar, G.M. (2007) 'Intelligent power management strategy of hybrid distributed generation system', *International Journal of Electric Power Energy System*, Vol. 29, pp.783–795.

Anderson, P.M. and Bose, A. (1983) 'Stability simulation of wind turbine systems', *IEEE Transactions on Power Apparatus and Systems*, Vol. PAS-102, No. 12, pp.3791–3795.

Benchouia, M.T., Ghadbane, I., Golea, A., Srairi, K. and Benbouzid, M.E.H. (2015) 'Implementation of adaptive fuzzy logic and PI controllers to regulate the DC bus voltage of shunt active power filter', *Applied Soft Computing*, Vol. 28, pp.125–131.

Bhattacharya, S. and Divan, D. (1995) 'Design and implementation of a hybrid series active filter system', in *26th Annual IEEE Power Electronics Specialists Conference, 1995. PESC'95 Record*, 18–22 June 1995, Atlanta, GA, USA, Vol. 1, No. 1, pp.189–195.

Cardenas, V., Moran, L., Bahamondes, A. and Dixon, J. (2003) 'Comparative analysis of real time reference generation techniques for four-wire shunt active power filters', in *PESC'03: IEEE 34th Annual Power Electronics Specialist Conference, 2003*, 15–19 June 2003, Acapulco, Mexico, Vol. 2, No. 1, pp.791–796.

Chaoui, A., Gaubert, J-P., Krim, F. and Rambault, L. (2008) 'On the design of shunt active filter for improving power quality', in *2008 IEEE International Symposium on Industrial Electronics*, 30 June–2 July 2008, Cambridge, UK, Vol. 1, No. 1, pp.31–37.

Chen, Y-M., Cheng, C-S. and Wu, H-C. (2006) 'Grid-connected hybrid PV/Wind power generation system with improved DC bus voltage regulation strategy', in *APEC'06: Twenty-First Annual IEEE Applied Power Electronics Conference and Exposition, 2006*, 19–23 March 2006, Dallas, TX, USA, Vol. 1, No. 1, pp.1088–1094.

Chen, S., Lai, Y.M., Tan, S.C. and Tse, C.K. (2007) 'Analysis and design of repetitive controller for harmonic elimination in PWM voltage source inverter systems', *IET Power Electronics*, Vol. 1, No. 4, pp.497–506.

Fukuda, S. and Yoda, T. (2001) 'A novel current-tracking method for active filters based on a sinusoidal internal model for PWM inverters', *IEEE Transactions on Industry Applications*, Vol. 37, No. 3, pp.888–895.

Ghamri, A., Mahni, T., Benchouia, M.T., Srairi, K. and Golea, A. (2015) 'Comparative study between different controllers used in three-phase four-wire shunt active filter', *Energy Procedia, Elsevier*, Vol. 74, pp.807–816.

Gow, J.A. and Manning, C.D. (1996) 'Development of a model for photovoltaic arrays suitable for use in simulation studies of solar energy conversion systems', in *Proceedings of the 6th International Conference on Power Electronics and Variable Speed Drives, 1996*, 23–25 September 1996, Nottingham, UK, Vol. 1, No. 1, pp.69–74.

Ingram, D.M.E. and Round, S.D. (1997) 'A novel digital hysteresis current controller for an active power filter', in *Proceedings of International Conference on Power Electronics and Drive Systems*, 26–29 May 1997, Singapore, Vol. 2, No. 1, pp.744–749.

Jayasankar, V.N. and Vinatha, U. (2016) 'Implementation of adaptive fuzzy controller in a grid connected wind-solar hybrid energy system with power quality improvement features', in *2016 Biennial International Conference on Power and Energy Systems: Towards Sustainable Energy (PESTSE)*, 21–23 January 2016, Bangalore, India, Vol. 1, No. 1, pp.1–5.

Jayasankar, V.N., Gururaj, M.V. and Vinatha, U. (2016) 'A study on hybrid renewable energy source interface to the non-ideal grid at distribution level with power quality improvements', in *IEEE 6th International Conference on Power Systems (ICPS), 2016*, 4–6 March 2016, New Delhi, India, Vol. 1, No. 1, pp.1–5.

Jeong, S-G. and Woo, M-H. (1997) 'DSP-based active power filter with predictive current control', *IEEE Transactions on Industrial Electronics*, Vol. 44, No. 3, pp.329–336.

Malesani, L., Mattavelli, P. and Buso, S. (1998) 'Dead-beat current control for active filters', in *Proceedings of the 24th Annual Conference of the IEEE Industrial Electronics Society, 1998 (IECON'98)*, 31 August–4 September 1998, Aachen, Germany, Vol. 3, No. 1, pp.1859–1864.

Mikkili, S. and Panda, A.K. (2011) 'Instantaneous active and reactive power and current strategies for current harmonics cancellation in 3-ph 4-Wire SHAF with both PI and fuzzy controllers', *Energy and Power Engineering*, Vol. 3, pp.285–298.

Villalva, M.G., Gazoli, J.R. and Filho, E.R. (2009) 'Comprehensive approach to modeling and simulation of photovoltaic arrays', *IEEE Transactions on Power Electronics*, Vol. 24, No. 5, pp.1198–1208.

Wang, G-D., Wai, R-J. and Liao, Y. (2012) 'Design of backstepping power control for grid-side converter of voltage source converter-based high-voltage dc wind power generation system', *IET Renewable Power Generation*, Vol. 7, No. 2, pp.118–133.

Yavari, M., Sabahi, M. and Babaei, E. (2012) 'Enhancement of instantaneous power theory under unbalanced grid voltages condition using positive sinusoidal signal regulator', in *IEEE 5th India International Conference on Power Electronics (IICPE)*, 6–8 December 2012, New Delhi, India, Vol. 1, No. 1, pp.1–6.